Supplement of Atmos. Chem. Phys., 23, 4489–4500, 2023
https://doi.org/10.5194/acp-23-4489-2023-supplement

Atmospheric Chemistry and Physics
Open Access
EGU

Supplement of

Measurement report: Radiative efficiencies of $(CF_3)_2CFCN$, CF_3OCFCF_2, and $CF_3OCF_2CF_3$

Beni Adi Trisna et al.

Correspondence to: Jeongsoon Lee (leejs@kriss.re.kr) and Jeong Sik Lim (lim.jeongsik@kriss.re.kr)

S1. Curve-of-growth measurement for optical pass length calibration of multipass cell

The N_2O in N_2 mixture flowed to the multipass cell at different N_2O partial pressures ranging between 0.0015 and 0.048 Torr. The mixture was prepared by mixing a high purity N_2O (99.9999%) with a high purity N_2 (99.9999%) using a precision gas mixer (Sonimix 2106). The mixing ratio of N_2O was set at 0.07969 ± 0.00016 cmol/mol. The gas mixture filled the cell between 1.9 and 60.1 Torr which was measured using a calibrated pressure gauge (MKS 626A13TBE). The data acquisition parameters were the same as those used for the OPL calibration measurements (Table 1). The only exception was the size of the aperture, which was set at 4 mm to increase the SNR at lower partial pressure measurements.

Absorption spectra were recorded at various N_2O partial pressures. The spectral absorption $A(\tilde{\nu})$ is $-\ln(\Phi(\tilde{\nu})/\Phi_0(\tilde{\nu}))$, where $\Phi(\tilde{\nu})$ and $\Phi_0(\tilde{\nu})$ are the transmitted and incident radiant powers, respectively. Subsequently, the ILS were deconvoluted by applying the ILS deconvolution procedure using home-written code, namely multispectrum fitting. In this code, the nonlinear least-squares (NLS) method was applied. The model function was the Voigt profile defined by $V(\tilde{\nu}, \boldsymbol{a})$ with the coefficient vector $\boldsymbol{a}$ consisting of the transition wavenumber, peak intensity, Lorentzian width, and Doppler width. The model function of $V(\tilde{\nu}, \boldsymbol{a})$ was convoluted with the instrument lineshape $ILS(\tilde{\nu})$ to simulate the modelled spectra. The model function of $V(\tilde{\nu}, \boldsymbol{a})$ was rationally approximated from the real part of the complex probability function.[1] Then, the near-solution coefficient vector $\boldsymbol{a_0}$ was determined by minimizing the residual quantity between the measured and modeled spectra. Because the closed-form solution of the sum of squared residuals (SSR) does not exist, the trust-region-reflective (TRR) algorithm serves to minimize the SSR.[2] The TRR algorithm forces global convergence (via the steepest descent or negative curvature direction) and achieves fast local convergence (via the Newton step when it exists).

After obtaining the best-fit parameters for each transition peak, that is, the optimized transition wavenumber, peak intensity, Lorentzian width, and Doppler width, the pure gas spectrum $A_{pgs}(\tilde{\nu})$ was reconstructed from the optimized parameters. $A_{pgs}(\tilde{\nu})$ for each partial pressure is shown in Figure 2 of the main text (left, second row), which is obtained from the convolution of the Lorentzian and Doppler widths. The area under the $A_{pgs}(\tilde{\nu})$ was calculated using the trapezoidal rule:

$$\int_a^b f(x)dx \approx \sum_{k=1}^{N} \frac{f(x_{k-1})+f(x_k)}{2} \Delta x_k \quad \text{(S1)}$$

where the Δx_k denotes the grid spacing of the data. The accuracy of this approximation depends on the grid resolution. Therefore, the grid resolution of the wavenumber is increased to 100,000 vector wavenumbers for each peak. Thus, the total wavenumber grid for the four peaks is 400,000. This method was validated by comparing the integration results with Origin's peak analyzer and the integration tool. A negligible difference (5.1×10^{-6} %) was found between the two procedures.

S2. Uncertainty evaluation of optical path length calibration

Derivation of uncertainty model equations

The uncertainty of L_{MP} was estimated based on the general law of uncertainty propagation (LUP) using the model equation:

$$L_{MP} = \frac{T_{MP} \cdot P_{RC} \cdot L_{RC} \cdot A_{MP} \cdot S_{T,RC}}{T_{RC} \cdot P_{MP} \cdot A_{RC} \cdot S_{T,MP}} \quad \text{(S2)}$$

where *T, P, L, A,* and S_T are the temperature, pressure, optical path length, absorption, and reference-line strength, respectively. The subscripts RC and MP represent the reference and multipass cells, respectively.

The line strengths of reference and multipass cells are governed by the thermodynamic and quantum chemical properties of the molecules, which can be estimated by the following equation[3]:

$$S_T = \left(\frac{Q_{T_0}}{Q_T}\right) \cdot exp\left\{-h \cdot c \cdot \frac{E''}{k_B} \cdot \left(\frac{1}{T} - \frac{1}{T_0}\right)\right\} \cdot \frac{\left[1-exp\left\{-h \cdot c \cdot \left(\frac{\tilde{\nu}_0}{k_B \cdot T}\right)\right\}\right]}{\left[1-exp\left\{-h \cdot c \cdot \left(\frac{\tilde{\nu}_0}{k_B \cdot T_0}\right)\right\}\right]} \cdot S_0 = P_T \cdot S_0 \quad \text{(S3)}$$

where Q_{T_0} (5007.816 at standard temperature) and Q_T are the partition functions of the absorbing gas at a reference temperature T_0 (296 K) and measured temperature *T*, respectively. where h is Planck's constant, E'' is the ground state energy of the corresponding transition, $\tilde{\nu}_0$ is the transition wavenumber, and c is the speed of light. Substituting eq S3 into eq S2 yields:

$$L_{MP} = \frac{T_{MP} \cdot P_{RC} \cdot L_{RC} \cdot A_{MP} \cdot P_{T,RC} \cdot S_0}{T_{RC} \cdot P_{MP} \cdot A_{RC} \cdot P_{T,MP} \cdot S_0} \quad \text{(S4)}$$

According to LUP, the combined standard uncertainty of the calibration result *y*, designated as $u_c(y)$ is obtained from a first-order Taylor series approximation of $y = f(X_1, X_2, \ldots . X_N)$ which is given by[4]

$$u_c^2(y) = \sum_{i=1}^{N} \left(\frac{\partial f}{\partial x_i}\right)^2 u^2(x_i) + 2 \sum_{i=1}^{N-1} \sum_{j=1+1}^{n} \frac{\partial f}{\partial x_i} \frac{\partial f}{\partial x_J} u(x_i) \cdot u(x_j) \cdot \rho_{ij} \quad \text{(S5)}$$

where the terms regarding partial derivatives are sensitivity coefficients, $u(x_i)$ is the standard uncertainty associated with input estimate x_i, and the term $u(x_i) \cdot u(x_j) \cdot \rho_{ij}$ is the estimated covariance associated with input estimates x_i and x_j with Pearson correlation coefficient ρ_{ij}. In eq S1, only the reference line strength S_0 is perfectly and positively correlated ($\rho = 1$), whereas the other parameters are uncorrelated ($\rho = 0$). Thus, eq S4 can be derived as:

$$\begin{aligned} u_c^2(L_{MP}) = {} & \left(\frac{\partial L_{MP}}{\partial T_{MP}}\right)^2 u^2(T_{MP}) + \left(\frac{\partial L_{MP}}{\partial P_{RC}}\right)^2 u^2(P_{RC}) + \left(\frac{\partial L_{MP}}{\partial L_{RC}}\right)^2 u^2(L_{RC}) + \\ & \left(\frac{\partial L_{MP}}{\partial A_{MP}}\right)^2 u^2(A_{MP}) + \left(\frac{\partial L_{MP}}{\partial P_{T,RC}}\right)^2 u^2\left(P_{T,RC}\right) + \left(\frac{\partial L_{MP}}{\partial S_{0,RC}}\right)^2 u^2\left(S_{0,RC}\right) + \left(\frac{\partial L_{MP}}{\partial T_{RC}}\right)^2 u^2(T_{RC}) + \\ & \left(\frac{\partial L_{MP}}{\partial P_{MP}}\right)^2 u^2(P_{MP}) + \left(\frac{\partial L_{MP}}{\partial A_{RC}}\right)^2 u^2(A_{RC}) + \left(\frac{\partial L_{MP}}{\partial P_{T,MP}}\right)^2 u^2\left(P_{T,MP}\right) + \left(\frac{\partial L_{MP}}{\partial S_{0,MP}}\right)^2 u^2\left(S_{0,MP}\right) + \\ & 2 \frac{\partial L_{MP}}{\partial S_{0,RC}} \frac{\partial L_{MP}}{\partial S_{0,MP}} u\left(S_{0,RC}\right) \cdot u\left(S_{0,MP}\right) \cdot \rho_{S_{0,RC}\, S_{0,MP}} \end{aligned} \quad \text{(S6)}$$

Because the line strengths of the probed reference lines S_0 are the same for reference and multipass cells, the uncertainties from S_0 and the sensitivity coefficients were identical. The term $S_{T,MP}$ $(= P_{T,MP} \cdot S_0)$ in the denominator of eq S1 results in a negative sensitivity coefficient, leading $\frac{\partial L_{MP}}{\partial S_{0,RC}} = -\frac{\partial L_{MP}}{\partial S_{0,MP}}$. Because the corresponding correlation coefficient is positive and perfect, $\rho_{S_{0,RC}\, S_{0,MP}} = 1$, the uncertainties of the reference line strengths S_0 can be cancelled, namely $\left(\frac{\partial L_{MP}}{\partial S_0}\right)^2 u^2(S_0) + \left(\frac{\partial L_{MP}}{\partial S_0}\right)^2 u^2(S_0) - 2 \frac{\partial L_{MP}}{\partial S_0} \frac{\partial L_{MP}}{\partial S_0} u(S_0) \cdot u(S_0) = 0$. For the uncertainty due to the temperature-dependent prefactor P_T, although the sensitivity coefficients of reference and multipass cells were the same, the extents of temperature variations of reference and multipass cells were slightly different. Additionally, the

measurements were independent ($\rho = 0$). Thus, the uncertainty cannot be ignored. Hence, eq S6 becomes:

$$u_c^2(L_{MP}) = \left(\frac{\partial L_{MP}}{\partial T_{MP}}\right)^2 u^2(T_{MP}) + \left(\frac{\partial L_{MP}}{\partial P_{RC}}\right)^2 u^2(P_{RC}) + \left(\frac{\partial L_{MP}}{\partial L_{RC}}\right)^2 u^2(L_{RC}) +$$
$$\left(\frac{\partial L_{MP}}{\partial A_{MP}}\right)^2 u^2(A_{MP}) + \left(\frac{\partial L_{MP}}{\partial P_{T,RC}}\right)^2 u^2\left(P_{T,RC}\right) + \left(\frac{\partial L_{MP}}{\partial T_{RC}}\right)^2 u^2(T_{RC}) + \left(\frac{\partial L_{MP}}{\partial P_{MP}}\right)^2 u^2(P_{MP}) +$$
$$\left(\frac{\partial L_{MP}}{\partial A_{RC}}\right)^2 u^2(A_{RC}) + \left(\frac{\partial L_{MP}}{\partial P_{T,MP}}\right)^2 u^2\left(P_{T,MP}\right) \quad \text{(S7)}$$

Then dividing eq S6 with L_{MP}^2, yields:

$$ru^2(L_{MP}) = ru^2(T_{MP}) + ru^2(P_{RC}) + ru^2(L_{RC}) +$$
$$ru^2(A_{MP}) + ru^2\left(P_{T,RC}\right) + ru^2(T_{RC}) + ru^2(P_{MP}) + ru^2(A_{RC}) + ru^2\left(P_{T,MP}\right)^2 \quad \text{(S8)}$$

where *ru* denotes relative standard uncertainty, *e.g.* $ru(y) = \frac{u(y)}{y}$.

Uncertainties of fitted peak area and COG slope

In typical spectrum fitting, if the model function is appropriately selected and the minimizer finds the global minimum, the residuals are randomly distributed.[5] This causes the fit residuals to be distributed normally to be propagated toward the uncertainty of the fitted area and finally identical to a general case of parametric uncertainty evaluation with a known probability distribution function. In contrast, our result exhibited a W-shaped pattern in the residuals (Figure 1), implying unresolved systematic uncertainty. Based on the assumption that the Voigt profile is the best lineshape function for the measured line and that the algorithm error is negligible at the minimized SSR, the uncertainty of the area of the absorption line $u(A_{line})$ was regarded as a consequence of instrumental error (nonideal phase error and modulation efficiency), including the drift of the ILS. Therefore, uniform distribution with a boundary limited to the maximum deviation of the residuals should be applied to obtain the uncertainty value of the fitted area. Because a rectangular distribution results in the most conservative uncertainty among the known statistical distributions, this approach cannot underestimate the uncertainty of the fitted area.

The nonlinearities in the absorption area should be tested to determine a linearly responding regime to simplify the OPL calibration procedure. If comparison measurements are conducted in a linear region, OPL calibration can be accomplished by one-point

calibration, that is, the ratio method. The N_2O absorption burdens of reference and multipass cells differed by 7.6 times as shown in Figure 2. The curve-of-growth measurements showed that the reference and multipass cell measurements were within the linear region (Figure 2). However, the slope determined by the weighted least squares method was uncertain due to regression uncertainty.[5] To account for this, the relative standard uncertainty of the slope in the curve-of-growth ru_{slope} was added to the uncertainty of the area of the multipass cell $ru_{A_{MP}}$. The slope of the straight line was 6.96×10^{-6}, while the expanded uncertainty of the slope was 1.67×10^{-7}. Therefore, the estimated value of ru_{slope} is 1.2%. Finally, the uncertainties of the fitted area covering the measured four peaks were estimated to be $ru_{A_{RC}} = 0.13\%$ and $ru_{A_{MP}} = 1.2\%$, respectively for the reference cell and the multipass cell.

Uncertainty of line strengths of N_2O

In the wavenumber range 2217.4 – 2219.0 cm^{-1}, the rovibrational transitions belong to the common transition band of 1001←1000, yielding an identical value of E'' for each transition. The details of the referred line data are summarized in Table S2. The partition function of N_2O was taken from the HITRAN database, in which temperature and several partition functions resulted in a linear relationship of $\Delta Q \cong 22.850 \cdot \Delta T$ in the range of 291–300 K. In our study, the cell temperature varied within 297 ± 1 K and the probability distribution was assumed to be uniform. Therefore, the temperature-dependent prefactor P_T was evaluated based on the variation trend of the temperature and the resulting partition function term $(\frac{Q_{T_0}}{Q_{T_0}+\Delta Q})$. The uncertainty of the reference line strength was cancelled according to eq S6. The line strength was varied by varying the temperature-dependent prefactor, P_T. The temperature variation in the reference and multipass cells was measured separately, and the resulting distribution for both measurements was assumed to have a uniform distribution. For instance, the temperature variation for reference cell measurement is ranged from 295.9 K to 296.3 K, yielding that P_T ranged from 5015.12503 to 5015.28998 for R9e, from 5015.128395 to 5015.13457 for P7e, from 5015.124983 to 5015.29214 for R10e, and from 5015.128427 to 5015.13306 for P6e. The uncertainty of the temperature-dependent prefactor $u(P_T)$ are then estimated to be 7.69134×10^{-25}, 3.89870×10^{-25}, 8.26422×10^{-25}, and 2.58868×10^{-25} $cm^{-1}/(molec\cdot cm^{-2})$, respectively for each peak. The temperature variation of multipass cell measurement was in a slightly different range from 295.2 K to 296.2 K., which corresponds to 2.41165×10^{-24}, 1.22241×10^{-24},

2.59128×10^{-24}, and 8.11664×10^{-25} $cm^{-1}/(molec\cdot cm^{-2})$ respectively for each peak. A combination of those with correction factor 4 (for averaging) indicates that $u(P_T)$ is insignificant in reference and multipass cell measurements (only about 8.5×10^{-4} %).

Uncertainty of length of the reference cell

Mechanical measurements of the reference cell were performed using a caliper (resolution:0.01 mm) that was calibrated against the national gauge block standards maintained by the Korea Research Institute of Standards and Science (KRISS). Thus, the uncertainty of the length of the reference cell L_{RC} was combined with the measurement and the uncertainty of the gauge block, resulting in 20.01 ± 0.05 mm.

Uncertainty because of temperature and pressure measurements

The temperature measurements were performed by attaching resistance thermometers to the cells. In addition, a pressure transducer was used to measure the pressures of the multipass and reference cells. The uncertainty contribution consists of the calibration certificate as a B-type and the repeatability of measurements as an A-type, which was calibrated against a standard platinum resistance thermometer, and the pressure transducer was calibrated against a standard ultrasonic manometer in KRISS. Pressure gauges are traceable to the KRISS standards, whereas temperature sensors are traceable to NIST temperature fixed-point standards.

S3. Parametric evaluation of uncertainty of radiative efficiency value

According to eq 4 of the main text, it was assumed that the major uncertainty source of radiative efficiency originated from the absorption cross-section measurement. It should be noted that the uncertainty of the radiative forcing model was unknown. This aspect of the uncertainty evaluation of radiative efficiency might not be an issue for the comparison of radiative efficiency values reported by independent research groups because the new narrow band model (nNBM) is currently considered the *de facto* standard of the radiative forcing model.[6] The uncertainty in the ACS measurement propagates to the final uncertainty of the radiative efficiency. The uncertainty of the absorption cross-section measurement is composed of the uncertainty due to temperature $u(T)$, pressure $u(P)$, certified reference material $u(x)$, OPL of the multipass cell $u(L_{MP})$, and wavenumber-dependent responsivity drift $u_v(rd)$. However, for $u_v(rd)$, the wavelength dependence did not significantly change the radiative efficiency uncertainty, as discussed in the next section. According to the LUP, the combined relative standard uncertainty of the radiative efficiency can be estimated by:

$$ru^2(RE) = ru^2(L_{MP}) + ru^2(P) + ru^2(x) + ru^2(T) + 2 \cdot ru^2(rd) \quad \text{(S9)}$$

where *ru* is the relative standard uncertainty. Uncertainty due to pressure, temperature, and certified reference material was evaluated in the same manner as in S2. For the uncertainty due to the OPL of the multipass cell, the value was taken from the calibration result of the cell in accordance with the evaluation given in S2.

Uncertainty of responsivity drift

The instrumental responsivity drift was evaluated for a measurement period of 1.5 h, because the baseline (I_0) fluctuated, as shown in Figure S2. Because the absorption cross-section measurement was not bracketed by consecutive single measurements of $\Phi_0(\tilde{\nu})$, the baseline of the absorption cross-section spectra fluctuated, affecting the integrated absorption cross-section values. It was found that the probability distribution of the $\Phi_{0,i}(\tilde{\nu})$ fluctuation in the measurement range of 500 – 3,000 cm^{-1} was normal. The relative standard uncertainty of instrumental responsivity $ru(rd)$ could be expressed as follows:

$$ru(rd) = \frac{\sqrt{\frac{\sum_{i=1}^{n}(R_{i,v}(\tilde{\nu}) - \bar{R}(\tilde{\nu}))^2}{n}}}{\bar{R}(\tilde{\nu})} \quad \text{(S10)}$$

where *n* is the number of measurements 18 for 1.5 h, which covered the entire measurement procedure of each absorption cross-section, assuming that $ru(rd)$ value was equivalent to that of the integrated absorption cross-section. This value was then combined as a B-type uncertainty with the standard uncertainty of the radiative efficiency (eq S9). The center spike in Figure S2 originates from the water absorption in the spectrometer. However, this strong signature did not affect the radiative forcing value.

Supplementary figures and tables

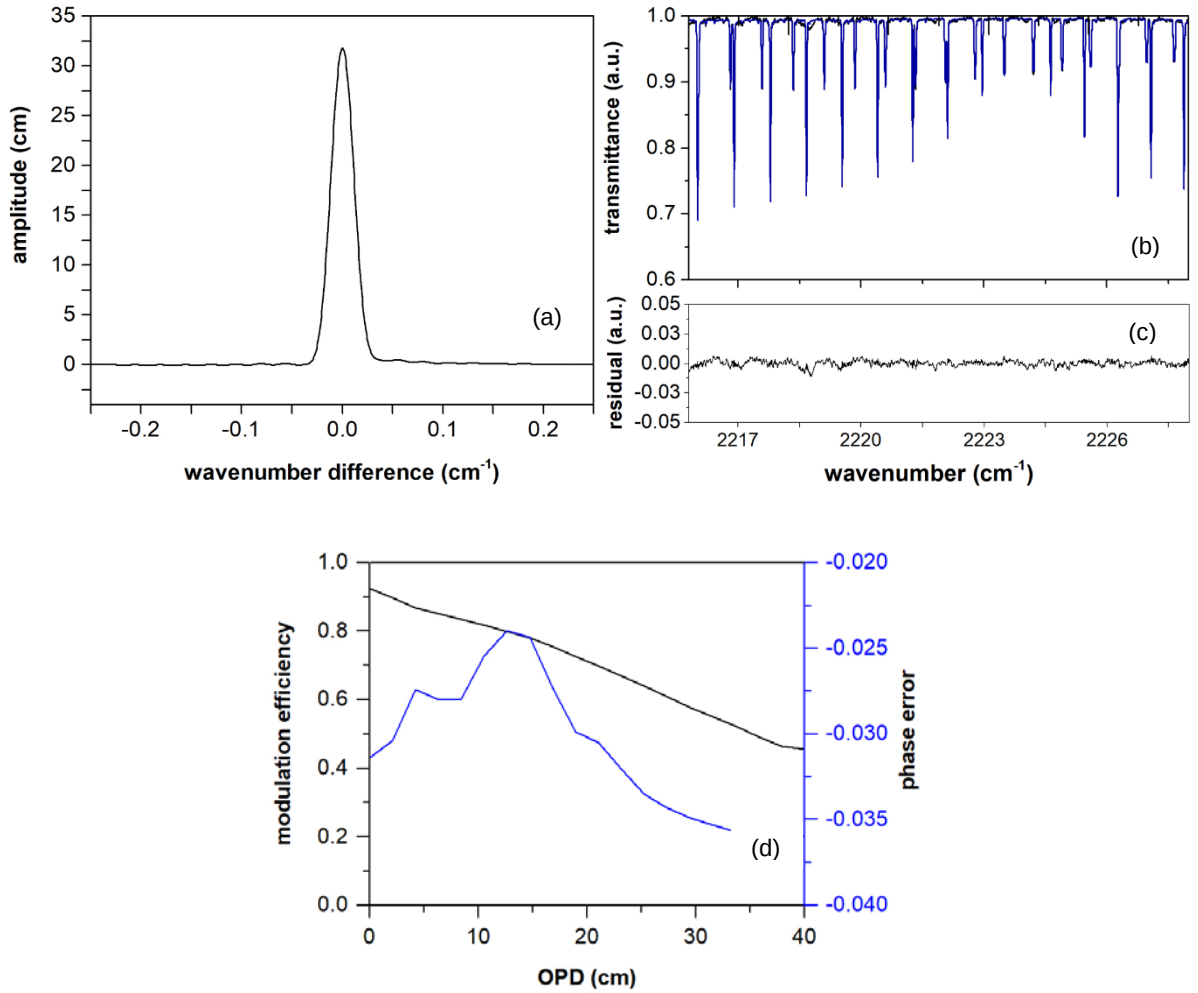

Figure S1 ILS reconstruction results from the N_2O spectrum. Reconstructed ILS (a) obtained using LINEFIT ver. 14 from the N_2O spectrum with reference cell as measured by the HR-FTIR (b). A fit of column amount (4.6016×10^{20} cm^{-2}) was superimposed with the measurement results in the wavenumber range of 2215–2228 cm^{-1}. Residuals are shown for the goodness of fit of the retrieved ILS (c). Phase error and modulation efficiency of the spectrometer (d).

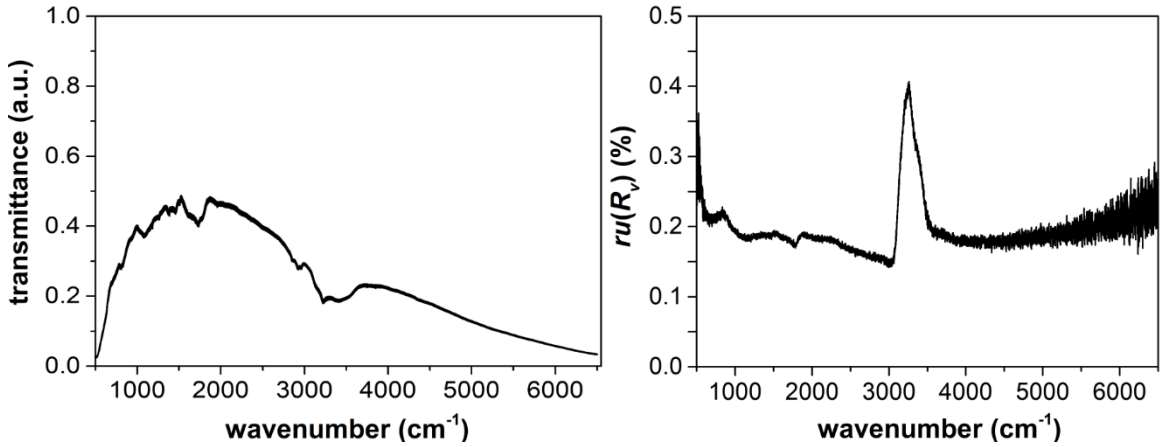

Figure S2 Responsivity drift measurement. Transmittance stability measurement is shown for 1.5 h (left), associated with the relative standard uncertainty of responsivity drift (right). The drift variation in the uncertainty plot is shown at 3200 cm^{-1}, which was caused by water vapor residues in the spectrometer body. However, the radiative forcing calculation model only considers the absorption band at 0 – 3,000 cm^{-1}; the uncertainty spiking is not included in the uncertainty calculation.

Table S1 Uncertainty budget of OPL calibration of the multipass cell. Values are displayed in relative (%).

Sources	Symbol	Relative Uncertainty (%), k=1	Sensitivity coefficient	DOF	Distribution	Type	Contribution (%)
Temperature of reference cell	$ru(T_{RC})$	0.19	-0.011	239	Uniform	A	2.4
Pressure of reference cell	$ru(P_{RC})$	0.14	0.034	4	Student's t	A	1.2
OPL of reference cell	$ru(L_{RC})$	0.12	160	99	Normal	A	0.9
Absorption (peak area) of reference cell	$ru(A_{RC})$	0.13	-110,000	705	Normal	A	0.8
Temperature of multipass cell	$ru(T_{MP})$	0.19	0.011	239	Uniform	A	2.4
Partial pressure of N_2O in multipass cell[1)]	$ru(P_{MP})$	0.08	-0.7	4	Student's t	A	0.4
Absorption (peak area) of multipass cell	$ru(A_{MP})$	1.2	14,000	449	Normal	A	91.9
Temperature dependent prefactor of multipass cell[2)]	$ru(P_{T,MP})$	4.92×10^{-4}	-6.3×10^{-4}	∞	Uniform	A	0
Temperature dependent prefactor of reference cell[2)]	$ru(P_{T,RC})$	4.94×10^{-4}	6.3×10^{-4}	∞	Uniform	A	0
Combined uncertainty	$ru(L_{MP})$	1.3	-	25,701	Normal	-	100

1) Combined uncertainty of total pressure and amount of N_2O in multipass cell

2) The temperature-dependent pre-factor P_T (transition assignment) for each cell was 5015.20750 (R9e), 5015.13148 (P7e), 5015.20856 (R10e), 5015.13074 (P6e), 5030.48421 (R9e), 5030.66897 (P7e), 5030.74628 (R10e), and 5030.66823 (P6e) for the reference cell and multipass cell, respectively.

Table S2 Referred line data for OPL calibration of the multipass cell. Data were taken from the HITRAN 2016.

Isotopologue	*v*	*S*	*A*	γ_{air}	γ_{self}	*E”*	Transition	*J’*	*J”*
$^{14}N_2{}^{16}O$	2217.53281	$4.677x10^{-20}$	97.31	0.0837	0.105	626.4924	R9e	10	9
$^{14}N_2{}^{16}O$	2217.74589	$6.330x10^{-19}$	113.5	0.087	0.109	23.4641	P7e	6	7
$^{14}N_2{}^{16}O$	2218.29598	$4.959x10^{-20}$	98.2	0.0824	0.104	634.8753	R10e	11	10
$^{14}N_2{}^{16}O$	2218.62524	$5.604x10^{-19}$	115.5	0.0881	0.11	17.5982	P6e	5	6

Table S3 Uncertainty budget of radiative efficiency value of NF_3.

Sources	Symbol	Relative uncertainty (%), k=1	Sensitivity coefficient $_i$	DOF	Distribution	Type	Contribution (%)
OPL of multipass cell	$ru(L_{MP})$	1.3	-6.2x10^{-4}	∞	Normal	B	38.33
Pressure	$ru(P)$	0.047	-5.5x10^{-4}	4	Student's t	A	0.05
Temperature	$ru(T)$	0.194	6.6x10^{-4}	∞	Uniform	A	0.93
Amount of substance	$ru(x)$	1.5	-2000	∞	Normal	B	55.19
Responsivity drift	$ru(rd)$	0.474	17	∞	Normal	B	5.51
Combined uncertainty	$ru(RE)$	2.02		∞	Normal	-	100

Table S4 Uncertainty budget of radiative efficiency value of SF_6.

Sources	Symbol	Relative uncertainty (%), k=1	Sensitivity coefficient $_i$	DOF	Distribution	Type	Contribution (%)
OPL of multipass cell	$ru(L_{MP})$	1.3	-1.8×10^{-3}	∞	Normal	B	85.06
Pressure	$ru(P)$	0.047	-5.0×10^{-3}	4	Student's t	A	0.12
Temperature	$ru(T)$	0.194	1.9×10^{-3}	∞	Uniform	A	2.06
Amount of substance	$ru(x)$	0.10	-11,000	∞	Normal	B	0.54
Responsivity drift	$ru(rd)$	0.474	100	∞	Normal	B	12.22
Combined uncertainty	$ru(RE)$	1.36		∞	Normal	-	100

Table S5 Uncertainty budget of radiative efficiency value of CF_4.

Sources	Symbol	Relative uncertainty (%), k=1	Sensitivity coefficient $_i$	DOF	Distribution	Type	Contribution (%)
OPL of multipass cell	$ru(L_{MP})$	1.3	-2.7×10^{-4}	∞	Normal	B	85.41
Pressure	$ru(P)$	0.047	-4.1×10^{-4}	4	Student's t	A	0.12
Temperature	$ru(T)$	0.194	2.9×10^{-4}	∞	Uniform	A	2.06
Amount of substance	$ru(x)$	0.05	-830	∞	Normal	B	0.14
Responsivity drift	$ru(rd)$	0.474	28	∞	Normal	B	12.27
Combined uncertainty	$ru(RE)$	1.35		∞	Normal	-	100

Table S6 Uncertainty budget of radiative efficiency value of PMVE.

Sources	Symbol	Relative uncertainty (%), k=1	Sensitivity coefficient $_i$	DOF	Distribution	Type	Contribution (%)
OPL of multipass cell	$ru(L_{MP})$	1.3	-1.0x10^{-3}	∞	Normal	B	38.33
Pressure	$ru(P)$	0.047	-7.0x10^{-4}	4	Student's t	A	0.05
Temperature	$ru(T)$	0.194	1.1x10^{-3}	∞	Uniform	A	0.93
Amount of substance	$ru(x)$	1.5	-3,300	∞	Normal	B	55.19
Responsivity drift	$ru(rd)$	0.474	13	∞	Normal	B	5.51
Combined uncertainty	$ru(RE)$	2.02		∞	Normal	-	100

Table S7 Uncertainty budget of radiative efficiency value of PFMEE.

Sources	Symbol	Relative uncertainty (%), k=1	Sensitivity coefficient $_i$	DOF	Distribution	Type	Contribution (%)
OPL of multipass cell	$ru(L_{MP})$	1.3	-1.7x10^{-3}	∞	Normal	B	38.33
Pressure	$ru(P)$	0.047	-7.1x10^{-3}	4	Student's t	A	0.05
Temperature	$ru(T)$	0.194	1.8x10^{-3}	∞	Uniform	A	0.93
Amount of substance	$ru(x)$	1.5	-1,100	∞	Normal	B	55.19
Responsivity drift	$ru(rd)$	0.474	15	∞	Normal	B	5.51
Combined uncertainty	$ru(RE)$	2.02		∞	Normal	-	100

Supplementary references

(1) Abrarov, S. M.; Quine, B. M. *J. Math. Res.* **2015**, *2*, 163-174.

(2) Kim, Y.; Lim, J. S. *Bull. Kor. Chem. Soc.* **2020**, *41*, 418-423.

(3) Allen, M. G. *Meas. Sci. Techn.* **1998**, *9*, 545.

(4) BIPM.; IEC.; IFCC., ILAC.; ISO.; IUPAC, IUPAP.; OIML. Evaluation of measurement data—guide for the expression of uncertainty in measurement. JCGM 100: 2008, JCGM 2008

(5) Tellinghuisen, J.; *Anal. Chem.* **2019**, *91*, 8715

(6) Hodnebrog, Ø.; Aamaas, B.; Fuglestvedt, J. S.; Marston, G.; Myhre, G.; Nielsen, C. J.; Sandstad, M.; Shine, K. P.; Wallington, T. J. *Rev. Geophys*. **2020**, *58*, e2019RG000691.